Enhanced Photocatalytic Activity of Agbr Photocatalyst via Constructing Heterogeneous Junctions With Reduced Graphene

Tongtong Zhang
Zhengzhou University
Qi Yin
University of Delaware
Menghan Zhang
Zhengzhou University
Siyu Zhang
Zhengzhou University
Yanning Shao
Zhengzhou University
Liyu Fang
Zhengzhou University
Qishe Yan (qisheyanzzu@163.com)
Institute of Chemistry and Molecular Engineering, Zhengzhou University https://orcid.org/0000-0002-9144-5659
Ximeng Sun
Zhengzhou University

Research Article

Keywords: rGO/AgBr, heterojunction, photocatalytic degradation, rhodamine B, composite photocatalyst

Posted Date: February 17th, 2021

DOI: https://doi.org/10.21203/rs.3.rs-229496/v1

Enhanced photocatalytic activity of AgBr photocatalyst via constructing heterogeneous junctions with reduced graphene

Tongtong Zhang[a] Qi Yin[b] Menghan Zhang[a] Siyu Zhang[a] Yanning Shao[a] Liyu Fang[a] Qishe Yan[a,*] Ximeng Sun[a,*]

[a] Green Catalysis Center, and College of Chemistry, Zhengzhou University, Zhengzhou, Henan, 450001, China

[b] Department of Chemistry & Biochemistry, College of Art and Science, University of Delaware, Newark, DE 19716 USA

[*] Corresponding author. E-mail and TEL: qisheyanzzu@163.com (Qishe Yan), sunximeng@zzu.edu.cn(Ximeng Sun), 037167781163

Abstract

A series of rGO/AgBr heterojunction photocatalysts were fabricated through a facile solvothermal method. The rGO/AgBr heterostructures were characterized by XPS, XRD, UV-Vis DRS, SEM, TEM, PL and the transient photocurrent responses. The XRD, SEM, XPS and TEM analyzes indicated that the graphene and silver bromide were successfully compounded without other impurities. The UV-Vis DRS exhibited that the composites have better optical properties than pure silver bromide. The PL and the transient photocurrent responses demonstrated that the addition of graphene significantly promotes the separation of photogenerated electrons and holes. Subsequently, the photocatalytic activities of rGO/AgBr composites were studied by degrading Rhodamine B (RhB). It turned out that the degradation rate of RhB by the rGO/AgBr heterojunction photocatalysts were significantly higher than that by pure AgBr. What's more, to study the photocatalytic degradation mechanism of RhB by rGO/AgBr heterostructures, the trapping experiments were used to identify the main active components. This work confirmed that the photocatalytic degradation performance of the catalyst was greatly improved after doping graphene, which provided certain data support for degradation of organic contaminants in water.

Keywords: rGO/AgBr, heterojunction, photocatalytic degradation, rhodamine B, composite photocatalyst

1. Introduction

Rapid industrial developments have improved human life quantity, whereas the discharge of pollution has become a compelling threat to the environment [1]. In recent years, enhancing the requirements of environmental protection, especially the treatment of sewage, which has a considerable impact on sustaining the development of human society. The organic dyes, which widely used in textile, printing, papermaking and other industries around the world, are colorants with complex structures, high molecular weight, water solubility, degradation resistance and potential carcinogenicity [2-4]. They will damage the aquatic ecosystem and threaten human health if the organic dyes in the wastewater are directly discharged into the rivers, lakes and groundwater. Therefore, the organic dyes in the wastewater have become a key issue for the pollution of water resources [1, 5]. In recent years, the requirements for environmental protection have been even higher, and the treatment of sewage has become a hot spot of social concern. Therefore, removing organic dyes in wastewater has become an urgent and significant research direction [3, 6]. Adsorption and chemical coagulation are techniques which often used in wastewater treatment. However, these techniques create secondary pollution [1, 7].

In order to degrade organic pollutants in water more effectively, photocatalysis, what is the most promising technology, has been studied by more and more researchers [8-11]. Among various semiconductor catalysts, titanium dioxide (TiO_2) has attracted the attention of researchers and extensive research has been carried out [12, 13]. However, TiO_2 has photocatalytic activity only under ultraviolet light, which accounts for about 2-5% of solar energy. Furthermore, the recombination of massive photogenerated electron holes limited its photocatalytic efficiency [12, 14]. Therefore, the discovery for new effective visible-light responsive photocatalysts is indispensable for future applications [8, 15].

Silver halide (AgX, X = Cl, Br, I),which is a photocatalytic material with a narrow band gap, exhibits great photocatalytic performances for organic pollutant removal in

the presence of visible light [11, 15-17]. However, pure AgX inevitably forms silver atoms under visible-light irradiation because its photogenerated electron tends to bond with an interstitial silver ions by absorbing incident light, and its photocatalytic efficiency will be inhibited by the photodecomposition [18-20]. As a consequence, the photo-induced stability of pure AgX could be improved by quickly capturing photo-generated electrons before they combining with silver ions to form silver atoms. [20]. Recently, it has been demonstrated that AgX can enhance stability and catalytic activity due to the formation of heterogeneous junctions by loading different cocatalysts [20-22]. For example, Chen et al. [23] synthesized AgBr/Ag_3PO_4@natural hematite heterojunction photocatalyst to degrade antibiotics under simulated solar light. In addition, Cao et al. [18] synthesized AgBr/WO_3 complex for the removal of methyl orange in visible light. Results indicated that the heterojunctions display outstanding performance than the single component, which may be due to the rapid separation of electron-hole pairs due to the existence of heterojunction structure [18, 24, 25]. Therefore, finding a suitable cocatalyst to form heterojunction with AgX is a research hotspot to improve photocatalytic performance. Recently, Graphene oxide (GO) and reduced graphene oxide (rGO) has drawn more and more attention from the researchers because of its high specific surface area and superior electron mobility [24, 26-28]. Now, the graphene oxide can be mass-produced at a lower cost, and there were so many researchers constructed plenty of different types of semiconductor-graphene (SC) heterojunction materials to improve their photocatalytic performance [17, 24], such as TiO_2/GO [29], Cu_2O/rGO [30], α-Fe_2O_3@GO [31], ZnO/rGO [32] and Bi_2WO_6/graphene [33]. As expected, the photocatalytic performances of the composites were improved because the graphene in the composites can promote charge separation and inhibit photo-generated electron-hole pair recombination.

Herein, series of rGO/AgBr heterojunction catalysts were processed via the simple solvothermal treatment. The photocatalytic properties of the rGO/AgBr hybrid materials were estimated by using RhB as a target organic pollutant, and the kinetics of photocatalytic degradation were studied. Furthermore, the photocatalytic

mechanism of rGO/AgBr complex was also investigated.

2. Experimental

2.1. Materials

All reagents were purchased from Kermel, and all of them were of analytical pure without further purification.

2.2. Synthesis of GO

GO was fabricated by modified Hummers method. First, a 1000ml flask was taked out, add 70 mL H_2SO_4 (98%), 3.0 g graphite powder and 1.5 g $NaNO_3$, and stir vigorously in an ice bath. With the vigorous stirring and the temperature at 0-4 degrees, 9 g $KMnO_4$ was added uniformly and slowly until the solution turned green. Then the beaker was magnetically stirred for 40min under the condition of oil bath (40 °C). Added 150 mL pure water to the above solution by inches and heated to 95°C for 15 minutes before removing the flask from the oil bath. The precipitation obtained by centrifugation was washed with hydrochloric acid (1:10) and pure water, then centrifuged for 30 min after 30 min of ultrasound, and the supernatant was retained and the precipitation (agglomerated GO) was removed. after that, ultrasonic and centrifuge (1000 r/min) again, and the solution was divided into three layers, Finally, the precipitation and supernatant were removed, the intermediate layer was retained. The concentration of GO was 0.007 g/mL.

2.3. Synthesis of rGO/AgBr

The rGO/AgBr composite photocatalysts were synthesized by facile solvothermal method and the experimental procedure is illustrated in Figure 1. First, 0.3397 g $AgNO_3$ was added to 20 mL ethylene glycol under magnetic stirring conditions. Then 0.265, 0.53, 0.802, 1.075 mL GO solution was added respectively, and the design was

0.5, 1, 1.5, 2% rGO/AgBr, respectively. In addition, the ethylene glycol solution of potassium bromide was added into the above dispersion, in which potassium bromide was excessive to ensure that there were enough halide ions to precipitate silver ions. After 30 mins magnetic stirring, the precursor solution was transferred into the Teflon-lined stainless steel autoclave and heated at 160 °C for 4 h. The obtained precipitation was washed with absolute ethanol and deionized water to remove ionic residue. Finally, the samples were dried at 60 °C and were denoted as rGO-A (A=0.5, 1, 1.5 and 2). The same process was used to prepare pure AgBr without the presence of GO.

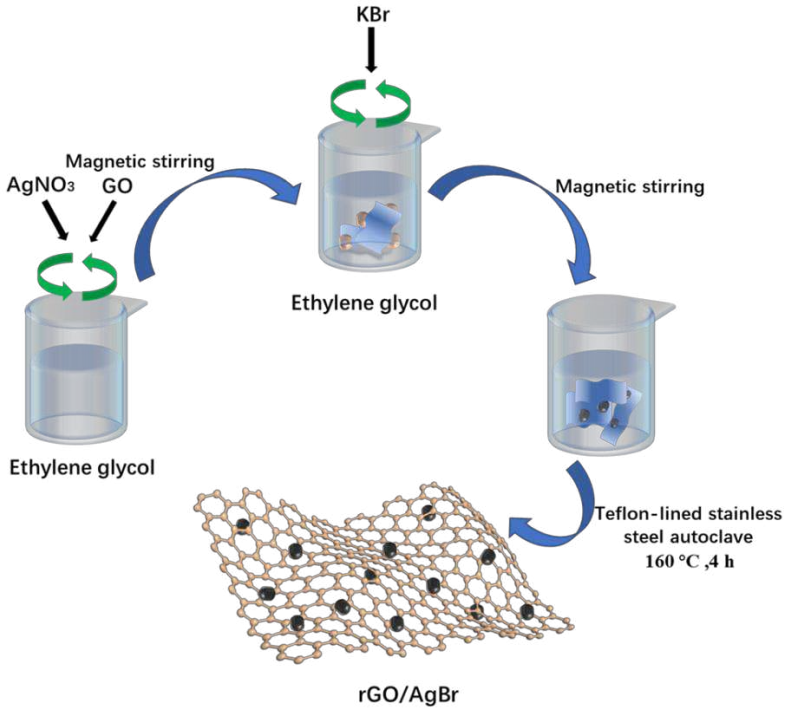

Scheme. 1. Preparation of rGO/AgBr composite material.

2.4. Characterization

The X-ray diffraction (XRD) patterns were identified by an X-ray diffractometer (D/MAX-r A, Rigaku, Japan). The morphologies of the samples were observed by scanning electron microscopy (SEM, Sigma 500, zeiss, Germany) and transmission electron microscope (TEM, TECNAIG2F20-S-TWIN, FEI, USA) with a field emission gun at 200 kV. The chemical compositions and valence state of the

composites were investigated by an X-ray photoemission spectroscopy (XPS, Thermo escalab 250Xi). UV-Vis diffuse reflection spectra (UV-Vis DRS) of the samples were performed by using a UV-Vis spectrophotometer (Caly 5000, Agilent, USA). Fourier-transform infrared spectra (FT-IR) were detected by FT-IR spectrophotometer (Nicolet iS50, Thermo, USA). The photoluminescence (PL) spectroscopy was measured at the excitation wavelength of 420 nm on F-4600 Fluorescence Spectrophotometer. Photoelectrochemical measurement was made on an electrochemical analyzer (CHI660E).

2.5. Photocatalytic experiments

The photocatalytic activity of the photocatalysts was determined by degradation of RhB solution (0.02 g/L) under 300 W xenon lamp ($\lambda \geq 420$ nm) irradiation. In the specific experiment, 0.05 g photocatalyst was added into 50ml RhB solution and stirred magnetically in the dark for 20 minutes to ensure the equilibrium of adsorption and desorption. During the irradiation process, 4 mL suspension was taken out at regular intervals (10 mins), and the catalyst was filtered out with 0.22 μm membrane filter, and the filtrate was determined by ultraviolet-visible spectrophotometer (UV-2450 Shimadzu, Japan). Photocatalytic performance can be described by the following equation:

$$D = C_t/\mathrm{C}_0 \times 100\%$$

Where D is the removal rate, C_0 and C_t are the initial concentration of RhB solution and the concentration after t min illumination respectively.

3. Results and discussions

3.1. Phase structure and morphology of photocatalysts

3.1.1. the structure characterization

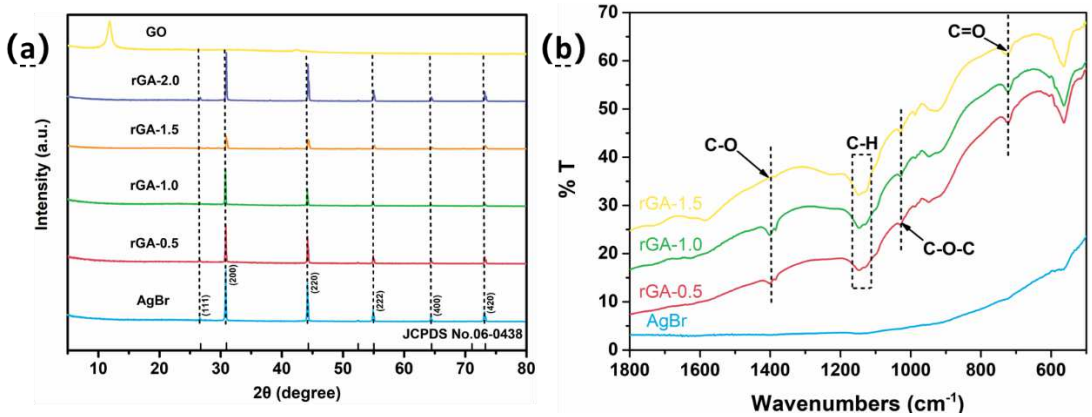

Fig. 1. (a) XRD patterns and (b) FT-IR spectra of GO, AgBr and rGA-A (A=0.5, 1, 1.5 and 2) composites.

The XRD patterns of GO, AgBr and rGO/AgBr composites with different rGO content were shown in Fig. 1a, which shown the crystal phase, purity and crystallinity of the prepared samples. The 2θ of AgBr were 26.725°, 30.960°, 44.346°, 55.042°, 64.476° and 73.261°, corresponding to (111), (200), (220), (222), (400) and (420) lattice planes of the cubic crystal (JCPDS 06-0438) [34]. And as can be seen in Fig. 1a, there were no characteristic peaks of GO and rGO in the composites, which may be due to the low content of GO. At the same time, no other impurity peaks were detected in all composite materials, which confirmed the high purity of AgBr and composites. In addition, all photocatalysts had sharp characteristic diffraction peaks, indicating that all catalysts had high crystallinity. In order to further prove the composition of the materials, FT-IR was used to verify the existence of characteristic chemical bonds, and thus prove the existence of rGO in the composite material. As shown in Fig. 1b, the typical peaks at 1400 cm^{-1}, 384 cm^{-1} and 723 cm^{-1} were corresponding to the C-O, C-O-C and C=O bonds. Compared with GO in the literature [11], the oxygen functional groups were fewer and weaker, which means that graphene oxide was reduced to reduced graphene during the preparation process.

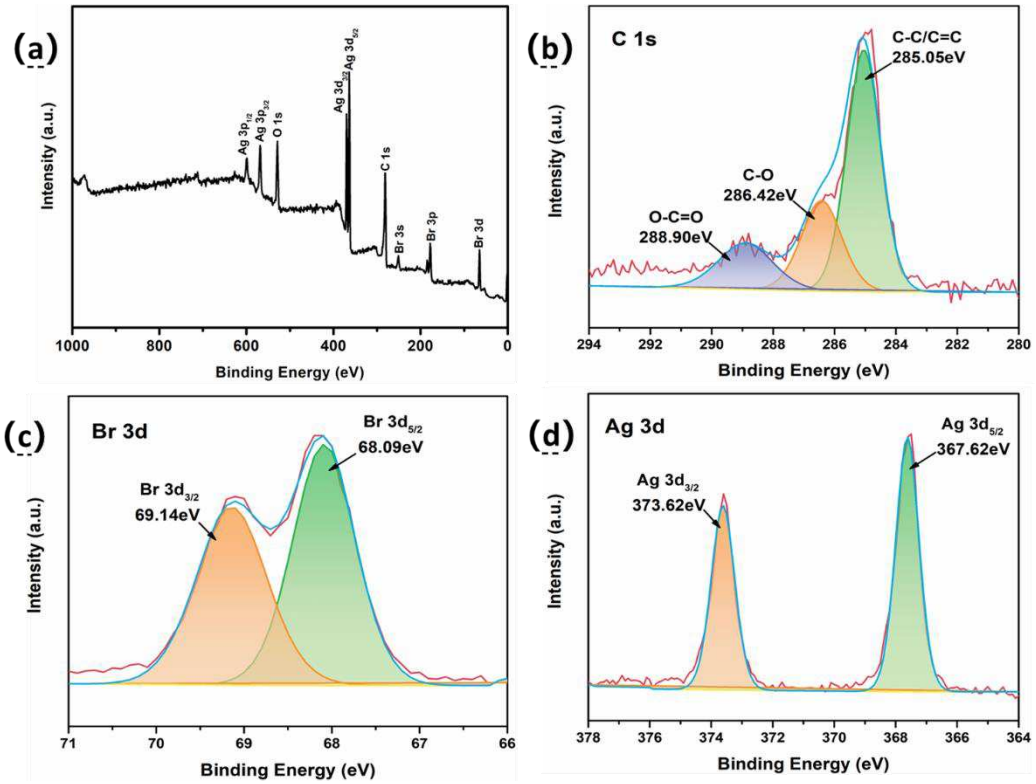

Fig. 2. XPS spectra of the rGA-1: (a) survey, (b) C 1s, (c) Br 3d, and (d) Ag 3d in rGA-1.

X-ray photoelectron spectroscopy was investigated to further study the element composition and chemical state of composite materials. From the complete spectrum shown in Fig. 2a, it can be seen that the elements on the surface of the material were Ag, Br, O, and C, corresponding to AgBr and rGO of the composite material, which meant successfully composited. In addition, the high-resolution spectra in Fig. 2(b-d) provided a clearer understanding of the chemical state of these elements. As shown in Fig. 2b, the three peaks of C 1s were 285.05eV, 286.42eV and 288.90eV, corresponding to C-C/C=C, C-O and O-C=O. The peak intensity of oxygen-containing functional groups was lower, that is, the content of oxygen-containing functional groups was less, which also proved that the graphene was reduced, which was the same as the FT-IR result shown in Fig. 1b. The peaks at 68.09eV and 69.14eV in Fig. 2c corresponded to Br $3d_{5/2}$ and Br $3d_{3/2}$ of Br 3d. In Fig. 2d, Ag 3d has characteristic peaks at 367.62eV and 373.62eV, corresponding to Ag $3d_{5/2}$ and Ag $3d_{3/2}$. It indicated that the catalyst of rGO/AgBr was successfully synthesized during the preparation process according to above analysis.

3.1.2. the morphology analysis

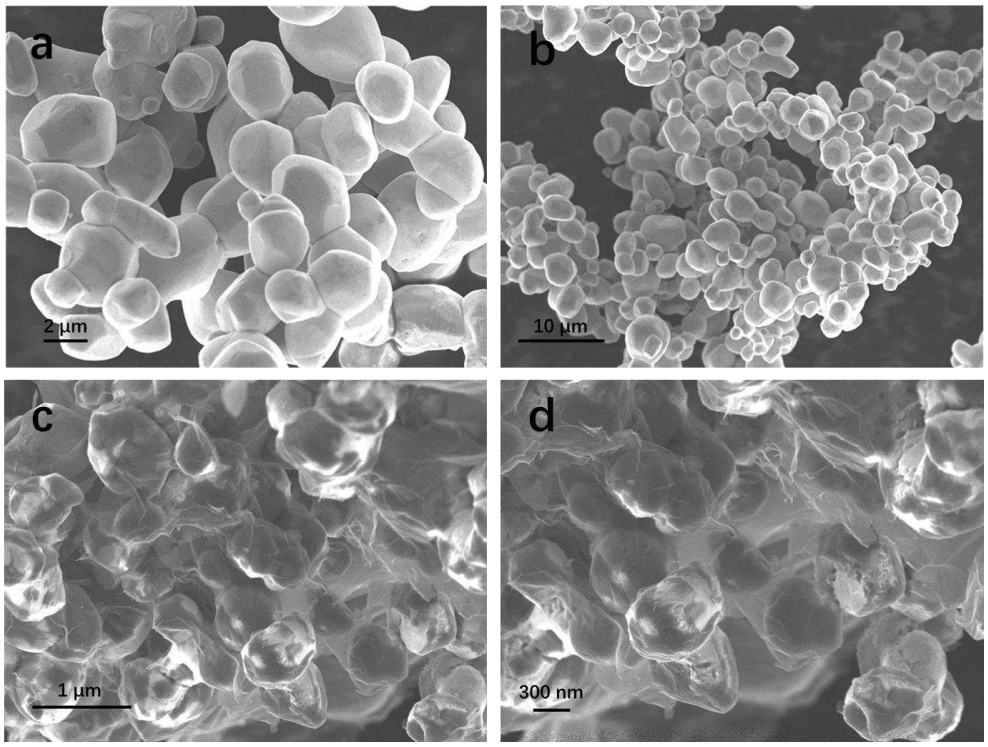

Fig. 3. SEM images of AgBr (a, b) and rGA-1(c, d).

The surface morphology of pure AgBr and rGA-1 samples were studied by SEM and TEM. Fig. 3a-b shown the SEM images of pure AgBr, indicating that the pure AgBr photocatalyst particles were irregular block morphology with uneven particle size and a diameter of about 1-4 μm. In addition, Fig. 3c-d shown the prepared rGA-1 sample composited with graphene. As shown in Fig. 3c, pure AgBr particles were uniformly covered by graphene, where the film-like substance was graphene. These figures shown that graphene has been successfully composited with pure AgBr photocatalyst. Compared with pure AgBr, after being composited with graphene, the diameter of AgBr was about 0.5-1.5μm, which were more uniform and smaller than pure AgBr particles. In contrast, the specific surface area was increased, and the contact area with pollutants was increased.

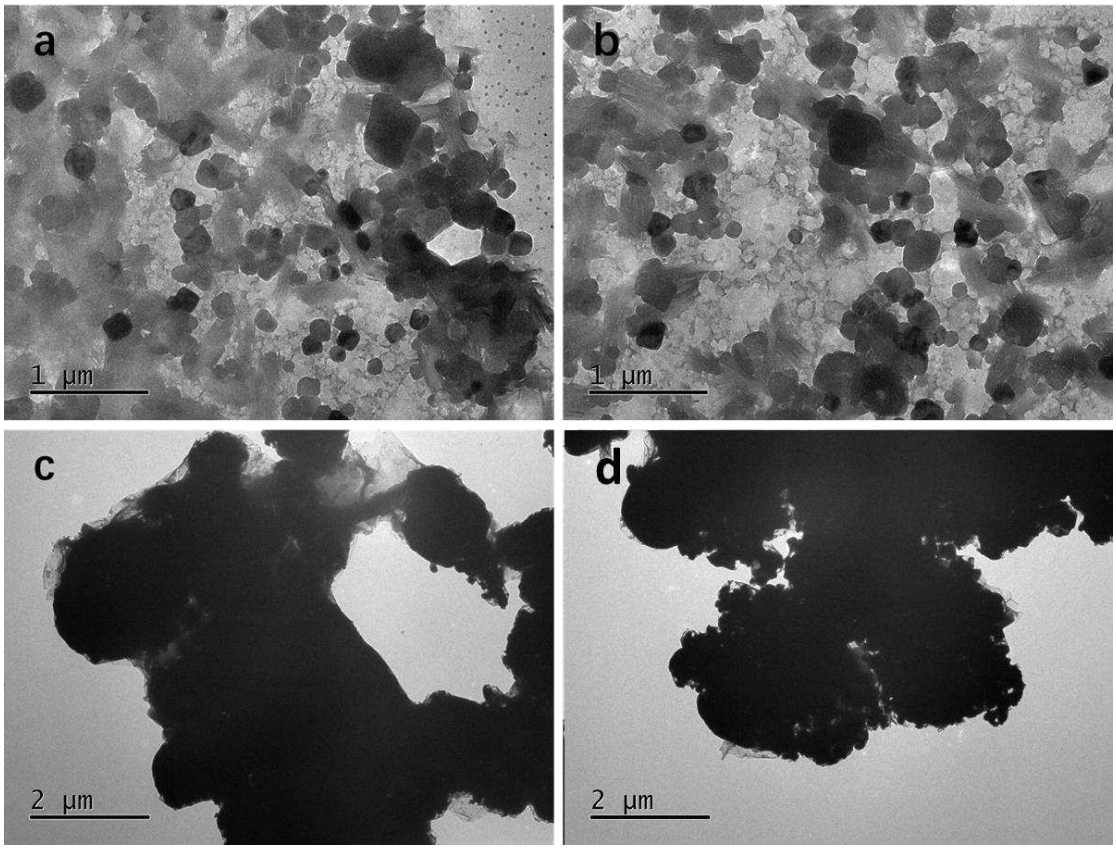

Fig. 4.TEM images of AgBr (a, b) and rGA-1(c, d).

TEM further shown the morphological characteristics of the samples. In Fig. 4a, AgBr particles were agglomerated block particles of uneven size. In Fig. 4c-d, after being composited with graphene, silver bromide was wrapped by graphene. It was evenly spread on the graphene, which may be due to the bonding of the oxygen-containing functional groups on the graphene to the silver particles. According to SEM and TEM, silver bromide particles were successfully loaded on graphene, thus, the two semiconductors were successfully combined.

3.2. The photoelectrochemistry properties of photocatalysts

3.2.1. Optical absorption property

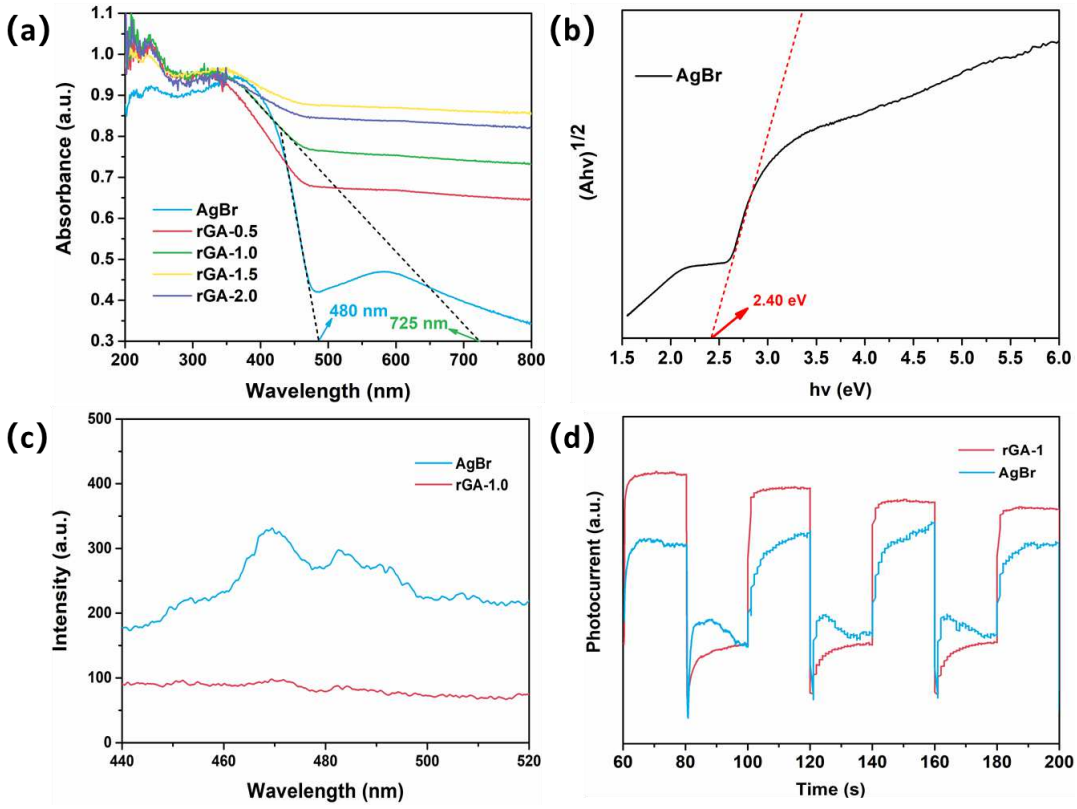

Fig. 5 (a) UV-vis diffuse reflectance spectra of AgBr and rGA-A (A=0.5, 1.0, 1.5 and 2.0) and (b) the bandgap of pure AgBr; (c) PL spectra of AgBr and rGA-A1.0; (d) Photocurrent response of AgBr and rGA-A1.0.

The optical properties of the different photocatalysts could be characterized by UV-Vis diffuse reflectance spectra, and the spectra of the as-prepared samples were demonstrated in Fig. 5a, which shown that the significant light absorption in visible range less than 480 nm was revealed by the pure AgBr. Whereas the spectra of the rGA-A (A=0.5, 1.0, 1.5 and 2.0) samples which contained graphene revealed the larger absorption edge visible light range and the wavelength had an obvious redshift. It shown that the rGO/AgBr photocatalyst exhibited the higher utilization efficiency of visible light than the pure AgBr photocatalyst. It was consistent with the results of photocatalytic degradation experiments, indicating that the enhancing the photocatalytic activity of AgBr composites attributes to the addition of GO in the photocatalysts. The bandgap energy of AgBr could be evaluated by the equation

mentioned below:

$$(\alpha h\nu)^{\frac{1}{n}} = A(h\nu - Eg)$$

In this equation, α, hv, A and Eg were the absorption coefficient, light frequency, a constant and bandgap energy. Furthermore, n depended on the type of semiconductor, the value of the direct bandgap semiconductor was 1/2 and the indirect band gap semiconductor was 2. According to previous review, AgBr was an indirect semiconductor, so that the value of n is 2. Thus, as shown in the Fig. 5b, it could be inferred that the Eg of AgBr was 2.40 eV.

3.2.2. Photoelectrochemistry properties

Photoluminescence spectra analysis can be used to analyze the separation efficiency of photoelectron and hole in photocatalyst. The combination of electron-hole pair will produce certain fluorescence intensity, the higher the combination rate of electron-hole pair is, the higher the fluorescence intensity is, and the worse the photocatalytic performance is. On the contrary, Low fluorescence intensity indicates better photocatalytic performance. For purpose of further exploring the influence of graphene on the catalytic performance of silver bromide, obtained catalysts were studied by photoluminescence spectra analysis. As shown in the Fig. 5c, the photoluminescence intensity of rGA-1 was significantly weaker than that of pure silver bromide when the excitation wavelength was 325 nm, indicating that the addition of graphene significantly inhibited the recombination rate of photocarriers and improved the separation efficiency of photogenerated electrons and holes, which was conducive to the improvement of photocatalytic activity.

Transient photocurrent responses spectroscopy was used to evaluate the efficiency of photoelectron separation and migration. For the transient photocurrent response results, high photoelectron separation efficiency is represented by high photocurrent intensity, which indicates good photocatalytic activity. The transient photocurrent responses diagram of AgBr and rGA-1 were displayed at the Fig. 5d. As shown in the figure, compared with pure AgBr, the photocurrent intensity of the composite was

stronger, indicating that the photoelectron separation efficiency of the composite was better, which further proved that the addition of graphene was conducive to photoelectron separation and transfer in catalyst, thus contributing to the improvement of photocatalytic efficiency. It was also in keeping with the previous PL results.

3.3. Photocatalytic activity

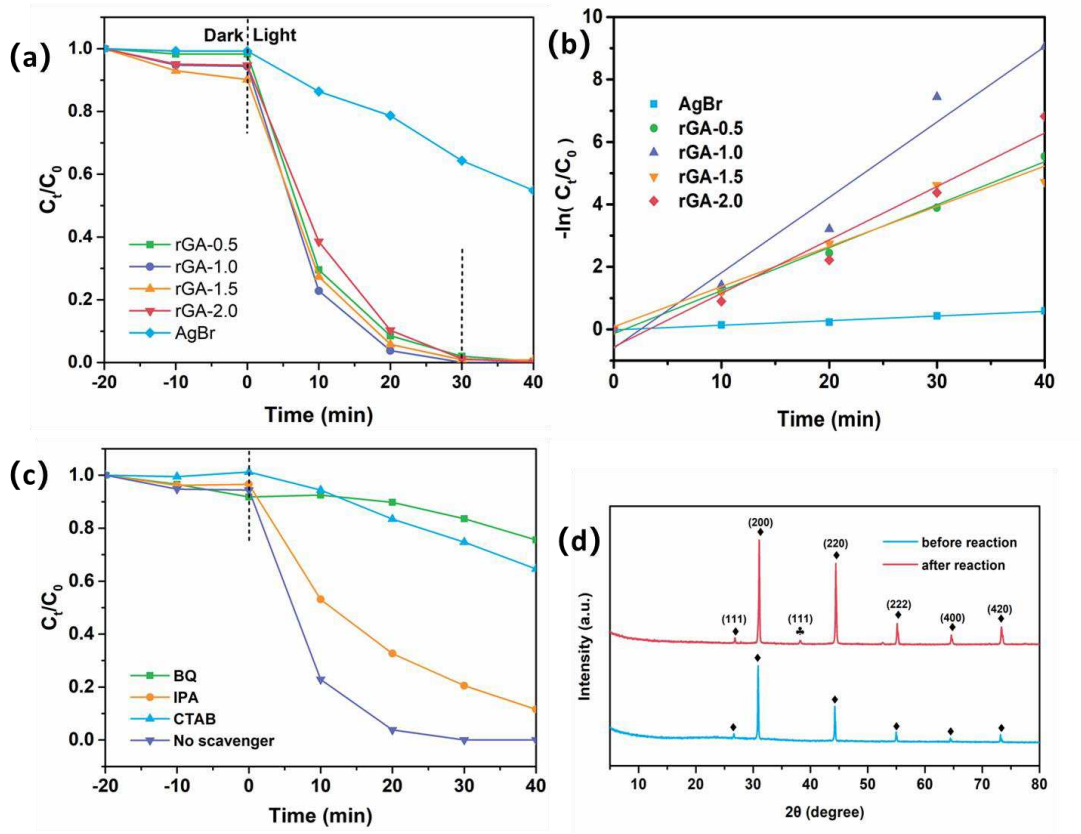

Fig. 6 (a) Photocatalytic degradation and (b) photocatalytic kinetics of RhB by the AgBr and rGA-A (A=0.5, 1.0, 1.5 and 2.0) composites under visible-light irradiation; (c) the trapping experiments of rGA-1.0; (d) XRD of rGA-1.0 after the photocatalysis experiment.

To determine the photocatalytic activity of the AgBr and a series of rGO/AgBr composites, RhB was used to investigate the photodegradation rate of these photocatalysts under the irradiation of a 300 W xenon lamp ($\lambda \geq 420$ nm). As shown in Fig. 6a, after 40 minutes irradiation from the xenon lamp, the degradation rate of rGA-0.5, rGA-1.0, rGA-1.5 and rGA-2.0 was almost 100.0%, while the degradation rate of AgBr was only 54.8%. which meant that compositing with rGO on the surface of AgBr improved the performance of photocatalyst. And the sample with the highest

degradation rate was rGA-1, which indicated that too much or too little rGO would affect the degradation efficiency. It may be that insufficient rGO leads to low electron transfer efficiency, while too much rGO may affect the visible light absorption and utilization of AgBr. Besides, too much rGO might form recombination centers, causing some electrons to recombine with holes on the surface of rGO.

To study the degradation rate of RhB by prepared catalysts, the kinetics of RhB degradation was studied by using a quasi-first-order kinetic model. The pseudo-first-order kinetic model:

$$-\ln(C_t/C_0) = k_{ap}t$$

Where C_t and C_0 represent the concentration of RhB at reaction time at t and 0; t and k_{ap} are the reaction time and the reaction rate constant, respectively. It can be seen from the Fig. 6b that the reaction rate constant of composite photocatalyst increased obviously compared with pure silver bromide. The rate constants k of rGA-0.5, rGA-1.0, rGA-1.5 and rGA-2.0 were 0.1377 min^{-1}, 0.2413 min^{-1}, 0.1287 min^{-1} and 0.1712 min^{-1}, respectively, which were twice of the pure silver bromide (0.0148 min^{-1}). It indicated that the photocatalytic degradation rate of AgBr composited with graphene was greatly increased. Among them, rGA-1.0 had the largest reaction rate.

3.4. Possible photocatalytic mechanism

In order to study the reaction mechanism in the photocatalytic degradation of RhB by rGA-1, the main active components generated in the degradation process were determined by trapping experiments. Here, p-benzoquinone (BQ), CTAB and isopropanol (IPA) were used as the scavengers for O_2^-, h^+ and •OH, respectively. As shown in the Fig. 6c, the photocatalytic degradation efficiencies of rGA-1.0 to RhB were significantly inhibited when BQ and CTAB were added, indicating that O_2^- and h^+ played major roles in degradation process. In addition, when IPA was added, the photocatalytic degradation rate of RhB by rGA-1 was partially reduced, indicating that •OH also played a role in the degradation process, but was not the main active substance in the degradation process.

In order to further study the possible photocatalytic degradation of organic pollutants by rGA-1 and the stability of the catalyst during the degradation process, XRD analysis was performed on the rGA-1 catalyst after the photocatalysis experiment. the characteristic peak at $2\theta = 38.116^{\circ}$ of the (111) crystal plane of metallic silver appeared after photocatalytic degradation, indicating that during the catalytic degradation process, rGA-1 produced a small amount of Ag under visible light. The surface plasmon resonance effect of these silver nanoparticles may contribute to the photocatalytic degradation of organic pollutants.

The CB energy level and the VB energy level of AgBr could be calculated according to the equation of the follow equation:

$$E_{VB} = E_{CB} + E_g$$

$$E_{CB} = X - E_c - 0.5E_g$$

Where E_{VB}, E_{CB}, X, E_c and E_g are the value band edge of semiconductor, the conduction band edge of semiconductor, the absolute electronegativity of the semiconductor. Therefore, the E_{CB} and the E_{VB} value of AgBr are 0.11 eV and 2.51 eV. Through the previous analysis and calculation, the possible photocatalytic mechanism for the photocatalytic degradation RhB by rGO/AgBr heterojunction photocatalyst was indicated in Scheme. 2.

First, under the irradiation of visible light, the electrons in the valence band of AgBr are excited and transferred to the conduction band, leaving holes in the valence band. At the same time, the metallic silver is excited by visible light, triggering the surface plasmon resonance effect. Usually, due to the narrow band gap, electron-hole pairs are rapidly recombinated, and only a small part of them participates in the photocatalytic process. However, due to the excellent performance of graphene's rapid photoelectron transfer, a large number of photogenerated electrons are transferred to rGO, which is combined with O_2 on the surface of rGO and converted into superoxide anion radicals. It has strong oxidation ability and can effectively degrade RhB adsorbed on rGO. In addition, due to electron transfer, the electrons and holes are separated and the holes remain in the valence band. The holes in the valence band that also have strong

oxidizing ability can directly oxidize and decompose the Rhodamine B adsorbed on the surface of the catalyst.

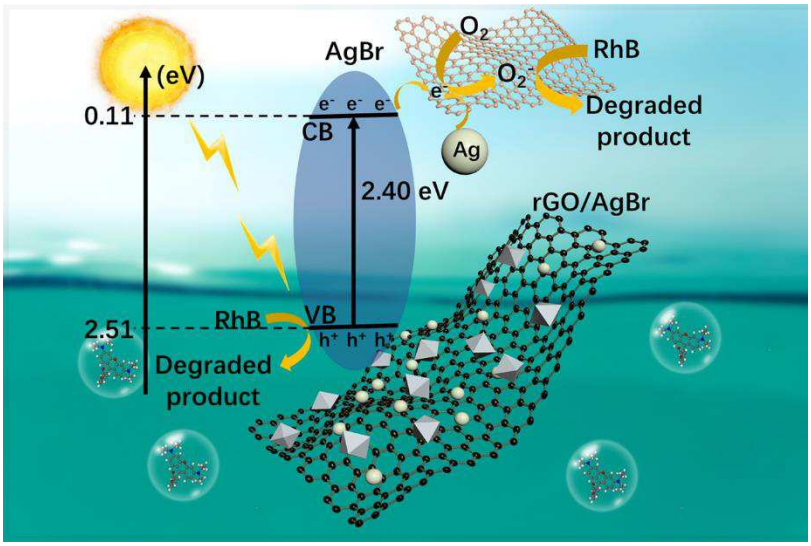

Scheme. 2 the possible photocatalytic mechanism for the photocatalytic degradation RhB by rGO/ AgBr photocatalyst.

4. Conclusion

The rGO/AgBr heterojunction photocatalysts, as the efficient visible-light-driven photocatalysts, were prepared by a facile solvothermal method. The graphene and silver bromide were successfully composited without other impurities, and the composites had better optical properties than pure silver bromide. The photocatalytic degradation experiment shown that the degradation rate of Rhodamine B by the rGO/AgBr photocatalysts (almost 100%) were significantly higher than that by pure AgBr (54.8%) after 40 minutes irradiation, identifying that compositing rGO on the surface of AgBr particles contribute to enhancing the photocatalytic activity. And the kinetics experiments shown that the degradation rate of 1% rGO/AgBr heterojunction catalysts was the highest, indicating that it is the most suitable for degrading Rhodamine B. Furthermore, the trapping experiments verified that the main active species in the photocatalytic degradation of organic pollutants by rGO/AgBr heterostructures were $\cdot O^{2-}$ and h^+. In brief, this experiment proved that the photocatalytic degradation rate of Rhodamine B in water was greatly improved after

compositing with GO, which was beneficial to the practical application of removing organic pollutants in water.

Acknowledgements

This work was supported by the Henan Provincial Department of Science and Technology (Grant No: 202102310266).

References

[1] S. Megala, S. Prabhu, S. Harish, M. Navaneethan, S. Sohila, R. Ramesh, Enhanced photocatalytic dye degradation activity of carbonate intercalated layered Zn, ZnNi and ZnCu hydroxides, Applied Surface Science, 481 (2019) 385-393.
[2] H. Veisi, S.B. Moradi, A. Saljooqi, P. Safarimehr, Silver nanoparticle-decorated on tannic acid-modified magnetite nanoparticles (Fe3O4@TA/Ag) for highly active catalytic reduction of 4-nitrophenol, Rhodamine B and Methylene blue, Materials science & engineering. C, Materials for biological applications, 100 (2019) 445-452.
[3] Gunture, A. Singh, A. Bhati, P. Khare, K.M. Tripathi, S.K. Sonkar, Soluble Graphene Nanosheets for the Sunlight-Induced Photodegradation of the Mixture of Dyes and its Environmental Assessment, Scientific reports, 9 (2019) 2522.
[4] S. Xue, C. Wu, S. Pu, Y. Hou, T. Tong, G. Yang, Z. Qin, Z. Wang, J. Bao, Direct Z-Scheme charge transfer in heterostructured MoO3/g-C3N4 photocatalysts and the generation of active radicals in photocatalytic dye degradations, Environmental pollution, 250 (2019) 338-345.
[5] T. Jiao, H. Guo, Q. Zhang, Q. Peng, Y. Tang, X. Yan, B. Li, Reduced Graphene Oxide-Based Silver Nanoparticle-Containing Composite Hydrogel as Highly Efficient Dye Catalysts for Wastewater Treatment, Scientific reports, 5 (2015) 11873.
[6] H. Xiao, W. Wang, G. Liu, Z. Chen, K. Lv, J. Zhu, Photocatalytic performances of g-C3N4 based catalysts for RhB degradation: Effect of preparation conditions, Applied Surface Science, 358 (2015) 313-318.
[7] J. Zhang, Z. Zhang, W. Zhu, X. Meng, Boosted photocatalytic degradation of Rhodamine B pollutants with Z-scheme CdS/AgBr-rGO nanocomposite, Applied Surface Science, 502 (2020).
[8] Q. Yan, X. Xie, C. Lin, Y. Zhao, S. Wang, Y. Liu, Synthesis of graphene oxide/Ag3PO4 composite with enhanced visible-light photocatalytic activity, Journal of Materials Science: Materials in Electronics, 28 (2017) 16696-16703.
[9] Y. Zhao, C. Lin, H. Bi, Y. Liu, Q. Yan, Magnetically separable CuFe2O4/AgBr composite photocatalysts: Preparation, characterization, photocatalytic activity and photocatalytic mechanism under visible light, Applied Surface Science, 392 (2017) 701-707.

[10] Q. Yan, M. Xu, C. Lin, J. Hu, Y. Liu, R. Zhang, Efficient photocatalytic degradation of tetracycline hydrochloride by Ag3PO4 under visible-light irradiation, Environmental Science and Pollution Research, 23 (2016) 14422-14430.
[11] Y. Yang, W. Zhang, R. Liu, J. Cui, C. Deng, Preparation and photocatalytic properties of visible light driven Ag-AgBr-RGO composite, Separation and Purification Technology, 190 (2018) 278-287.
[12] X. Xiao, L. Ge, C. Han, Y. Li, Z. Zhao, Y. Xin, S. Fang, L. Wu, P. Qiu, A facile way to synthesize Ag@AgBr cubic cages with efficient visible-light-induced photocatalytic activity, Applied Catalysis B: Environmental, 163 (2015) 564-572.
[13] M. Abd Elkodous, S.E.-S. G, M.I.A. Abdel Maksoud, R. Kumar, K. Maegawa, G. Kawamura, W.K. Tan, A. Matsuda, Nanocomposite matrix conjugated with carbon nanomaterials for photocatalytic wastewater treatment, J Hazard Mater, (2020) 124657.
[14] K. Kasinathan, J. Kennedy, M. Elayaperumal, M. Henini, M. Malik, Photodegradation of organic pollutants RhB dye using UV simulated sunlight on ceria based TiO2 nanomaterials for antibacterial applications, Scientific reports, 6 (2016) 38064.
[15] J. Chen, J. Zhu, Z. Da, H. Xu, J. Yan, H. Ji, H. Shu, H. Li, Improving the photocatalytic activity and stability of graphene-like BN/AgBr composites, Applied Surface Science, 313 (2014) 1-9.
[16] G. Chen, M. Zhu, X. Wei, Photocatalytic properties of attached BiOCl-(0 0 1) nanosheets onto AgBr colloidal spheres toward MO and RhB degradation under an LED irradiation, Materials Letters, 212 (2018) 182-185.
[17] P. Wang, Y. Cao, X. Zhou, C. Xu, Q. Yan, Facile construction of 3D hierarchical flake ball-shaped γ-AgI/Bi2WO6 Z-scheme heterojunction towards enhanced visible-light photocatalytic performance, Applied Surface Science, 531 (2020).
[18] J. Cao, B. Luo, H. Lin, S. Chen, Photocatalytic activity of novel AgBr/WO3 composite photocatalyst under visible light irradiation for methyl orange degradation, Journal of hazardous materials, 190 (2011) 700-706.
[19] D. Zhang, H. Tang, Y. Wang, K. Wu, H. Huang, G. Tang, J. Yang, Synthesis and characterization of graphene oxide modified AgBr nanocomposites with enhanced photocatalytic activity and stability under visible light, Applied Surface Science, 319 (2014) 306-311.
[20] H. Yu, L. Xu, P. Wang, X. Wang, J. Yu, Enhanced photoinduced stability and photocatalytic activity of AgBr photocatalyst by surface modification of Fe(III) cocatalyst, Applied Catalysis B: Environmental, 144 (2014) 75-82.
[21] Y. Fan, W. Ma, D. Han, S. Gan, X. Dong, L. Niu, Convenient recycling of 3D AgX/graphene aerogels (X = Br, Cl) for efficient photocatalytic degradation of water pollutants, Advanced materials, 27 (2015) 3767-3773.
[22] H. Xu, J. Yan, Y. Xu, Y. Song, H. Li, J. Xia, C. Huang, H. Wan, Novel visible-light-driven AgX/graphite-like C3N4 (X=Br, I) hybrid materials with synergistic photocatalytic activity, Applied Catalysis B: Environmental, 129 (2013) 182-193.
[23] L. Chen, S. Yang, Y. Huang, B. Zhang, F. Kang, D. Ding, T. Cai, Degradation of antibiotics in multi-component systems with novel ternary AgBr/Ag3PO4@natural hematite heterojunction photocatalyst under simulated solar light, Journal of hazardous materials, 371 (2019) 566-575.

[24] H. Wang, L. Zhang, Z. Chen, J. Hu, S. Li, Z. Wang, J. Liu, X. Wang, Semiconductor heterojunction photocatalysts: design, construction, and photocatalytic performances, Chemical Society reviews, 43 (2014) 5234-5244.
[25] H. Shen, M. Wang, X. Zhang, D. Li, G. Liu, W. Shi, 2D/2D/3D architecture Z-scheme system for simultaneous H2 generation and antibiotic degradation, Fuel, 280 (2020).
[26] X. Wang, Y. Liu, H. Pang, S. Yu, Y. Ai, X. Ma, G. Song, T. Hayat, A. Alsaedi, X. Wang, Effect of graphene oxide surface modification on the elimination of Co(II) from aqueous solutions, Chemical Engineering Journal, 344 (2018) 380-390.
[27] F. Chen, Q. Yang, S. Wang, F. Yao, J. Sun, Y. Wang, C. Zhang, X. Li, C. Niu, D. Wang, G. Zeng, Graphene oxide and carbon nitride nanosheets co-modified silver chromate nanoparticles with enhanced visible-light photoactivity and anti-photocorrosion properties towards multiple refractory pollutants degradation, Applied Catalysis B: Environmental, 209 (2017) 493-505.
[28] S. Yu, J. Wang, S. Song, K. Sun, J. Li, X. Wang, Z. Chen, X. Wang, One-pot synthesis of graphene oxide and Ni-Al layered double hydroxides nanocomposites for the efficient removal of U(VI) from wastewater, Science China Chemistry, 60 (2017) 415-422.
[29] L. Zhang, Q. Zhang, H. Xie, J. Guo, H. Lyu, Y. Li, Z. Sun, H. Wang, Z. Guo, Electrospun titania nanofibers segregated by graphene oxide for improved visible light photocatalysis, Applied Catalysis B: Environmental, 201 (2017) 470-478.
[30] Y.-C. Pu, H.-Y. Chou, W.-S. Kuo, K.-H. Wei, Y.-J. Hsu, Interfacial charge carrier dynamics of cuprous oxide-reduced graphene oxide (Cu2O-rGO) nanoheterostructures and their related visible-light-driven photocatalysis, Applied Catalysis B: Environmental, 204 (2017) 21-32.
[31] Y. Liu, W. Jin, Y. Zhao, G. Zhang, W. Zhang, Enhanced catalytic degradation of methylene blue by α-Fe2O3/graphene oxide via heterogeneous photo-Fenton reactions, Applied Catalysis B: Environmental, 206 (2017) 642-652.
[32] J. Qin, X. Zhang, C. Yang, M. Cao, M. Ma, R. Liu, ZnO microspheres-reduced graphene oxide nanocomposite for photocatalytic degradation of methylene blue dye, Applied Surface Science, 392 (2017) 196-203.
[33] Z. Zhu, Y. Ren, Q. Li, H. Liu, H. Weng, One-pot electrodeposition synthesis of Bi2WO6/graphene composites for photocatalytic applications under visible light irradiation, Ceramics International, 44 (2018) 3511-3516.
[34] J. Zhang, J. Dai, J. Chen, A comparative study in single- and binary-contaminant systems: the photodegradation of tetracycline and imidacloprid on flower-shaped Ag/AgBr/BiOBr under visible-light irradiation, New Journal of Chemistry, 44 (2020) 14180-14188.

Figures

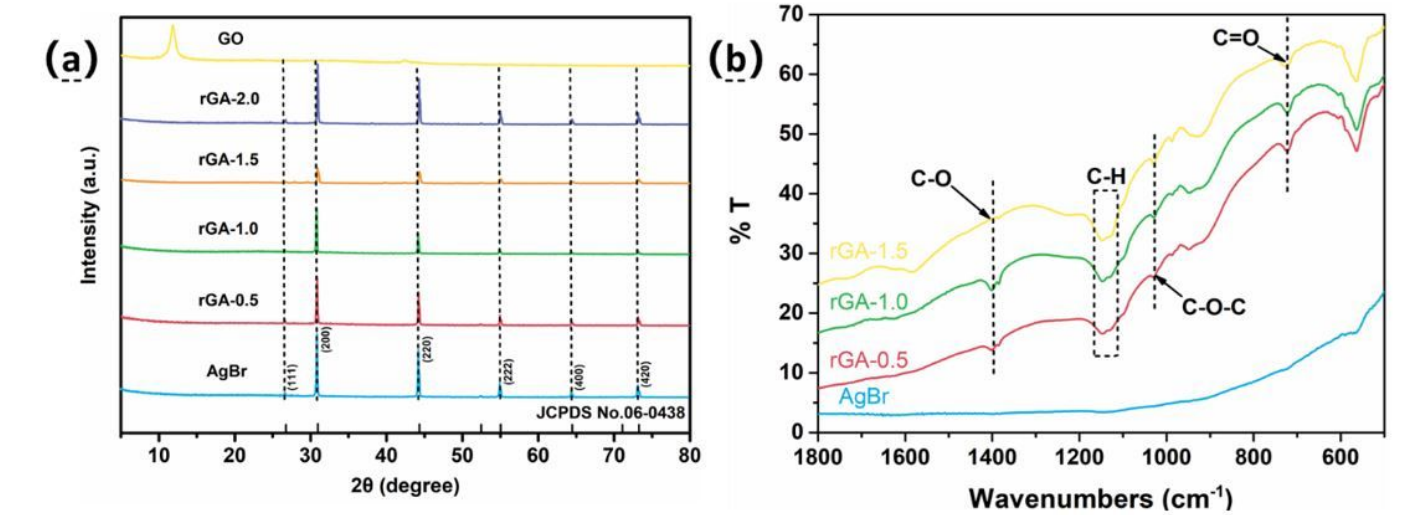

Figure 1

(a) XRD patterns and (b) FT-IR spectra of GO, AgBr and rGA-A (A=0.5, 1, 1.5 and 2) composites.

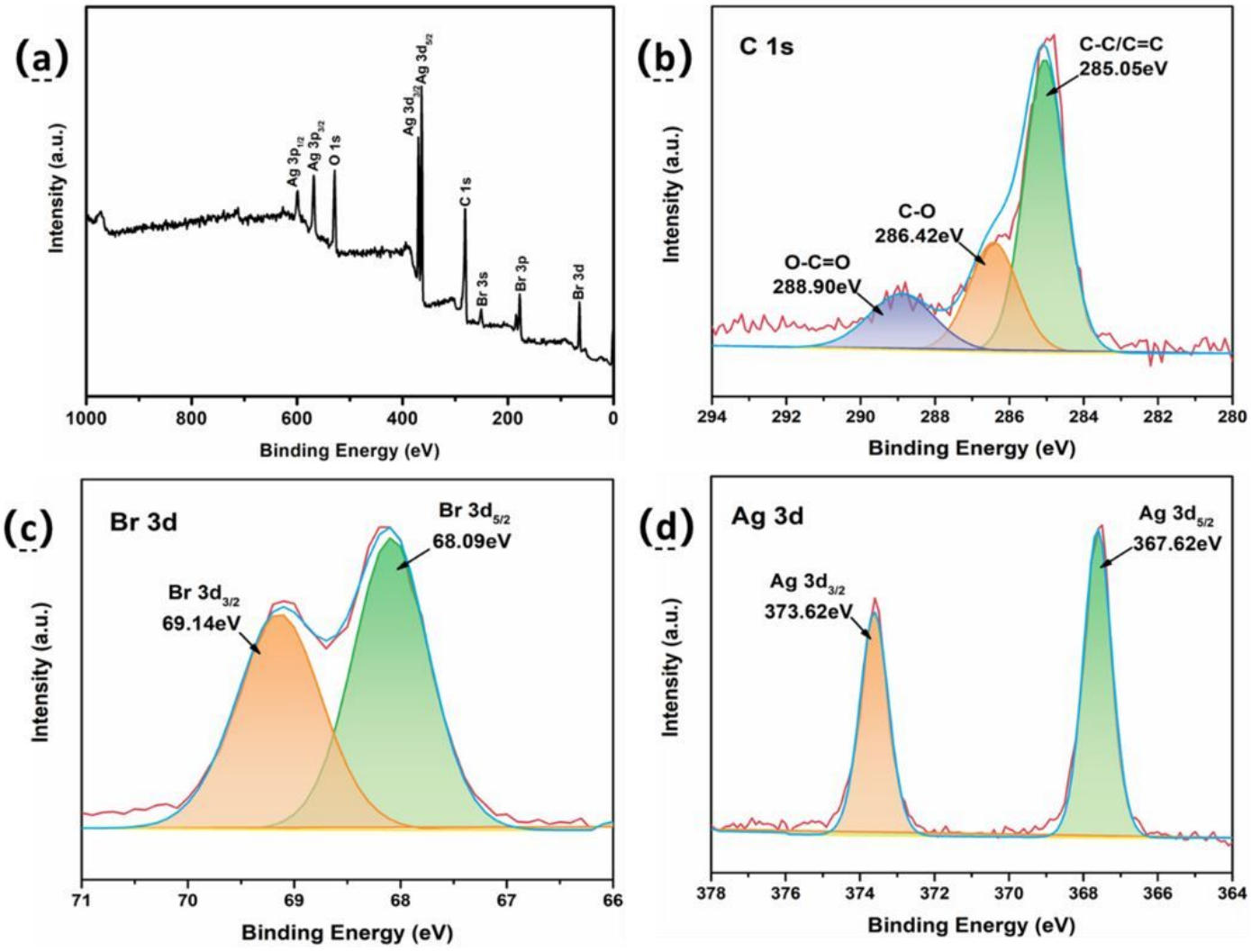

Figure 2

XPS spectra of the rGA-1: (a) survey, (b) C 1s, (c) Br 3d, and (d) Ag 3d in rGA-1.

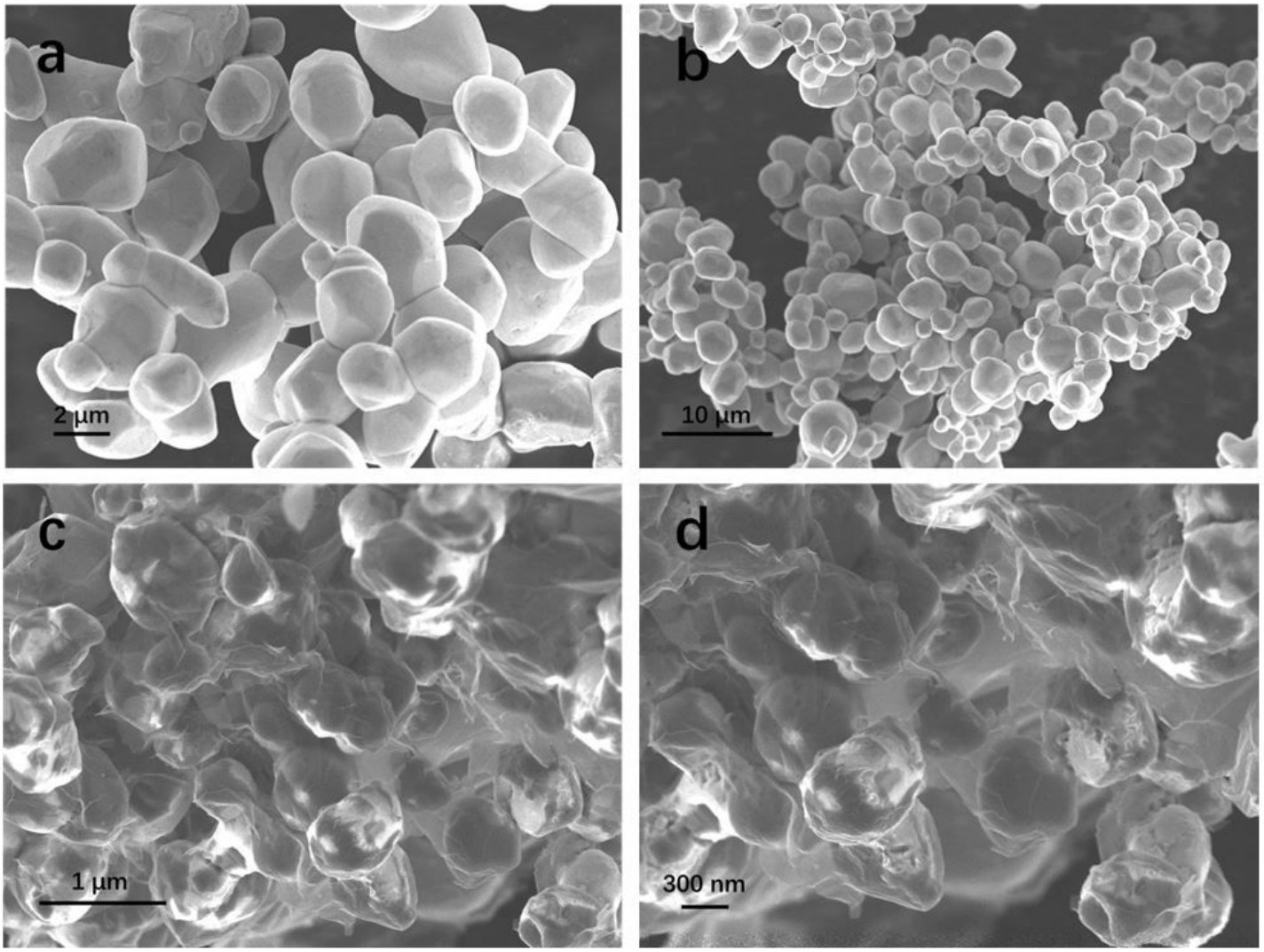

Figure 3

SEM images of AgBr (a, b) and rGA-1(c, d).

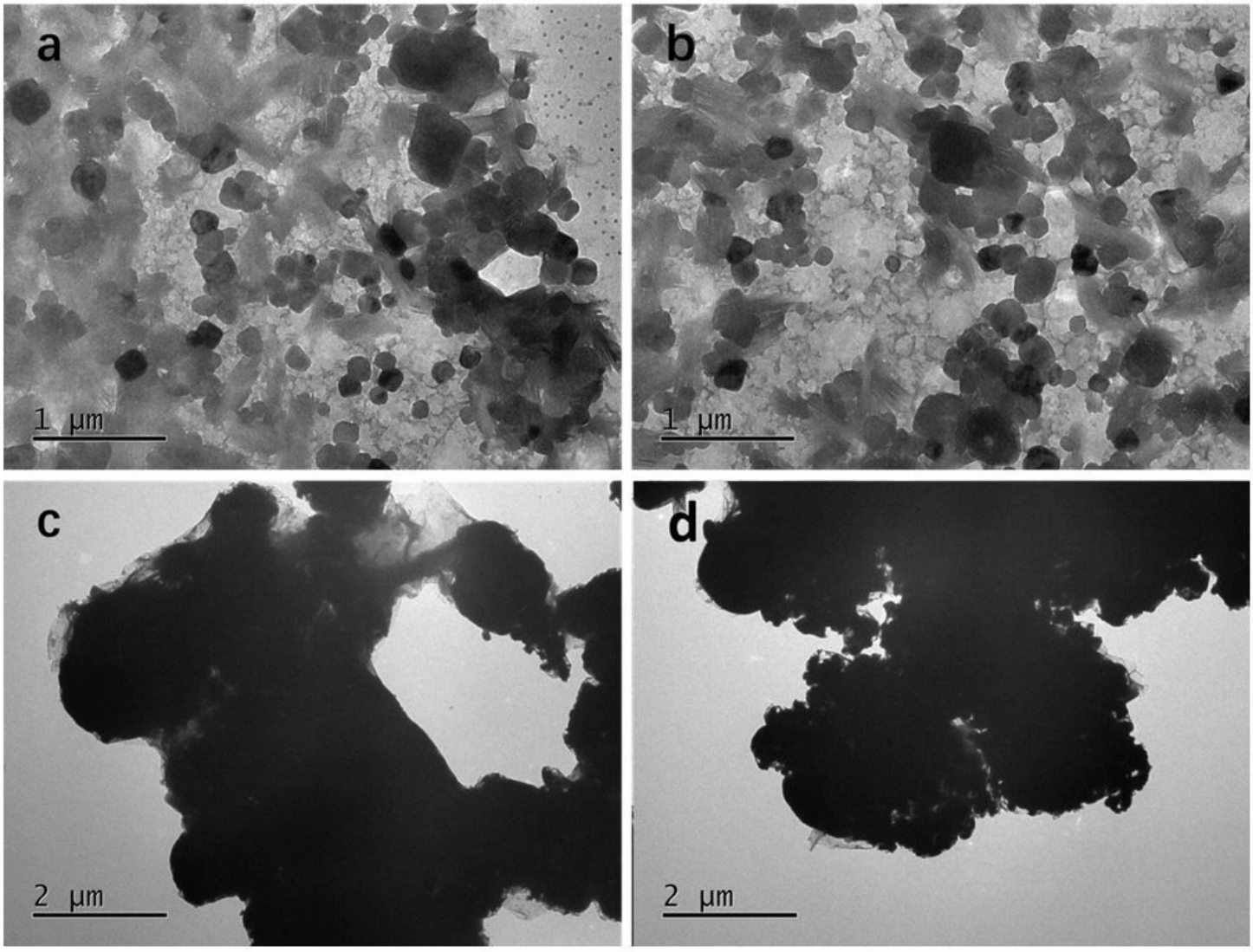

Figure 4

TEM images of AgBr (a, b) and rGA-1(c, d).

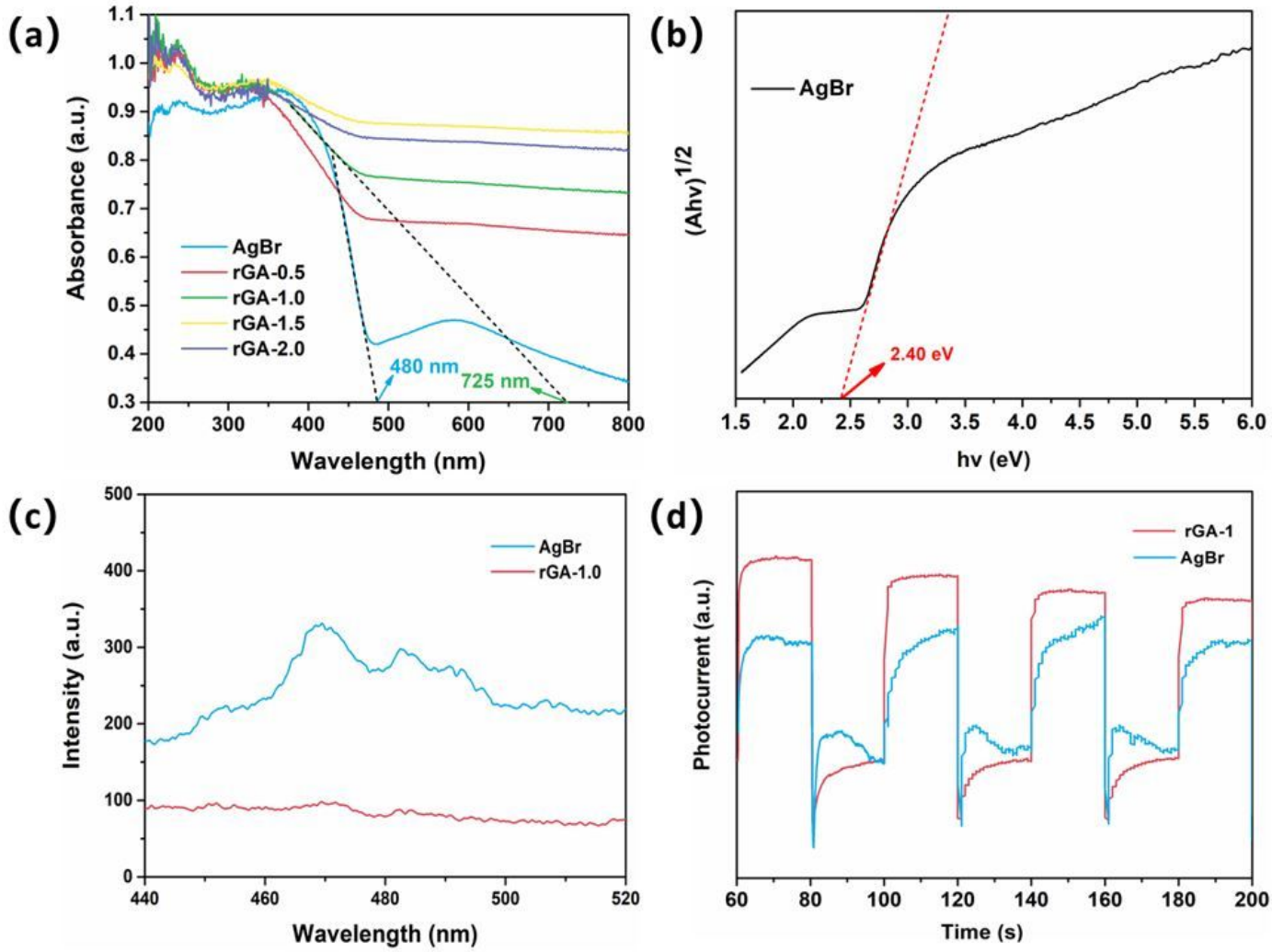

Figure 5

(a) UV-vis diffuse reflectance spectra of AgBr and rGA-A (A=0.5, 1.0, 1.5 and 2.0) and (b) the bandgap of pure AgBr; (c) PL spectra of AgBr and rGA-A1.0; (d) Photocurrent response of AgBr and rGA-A1.0.

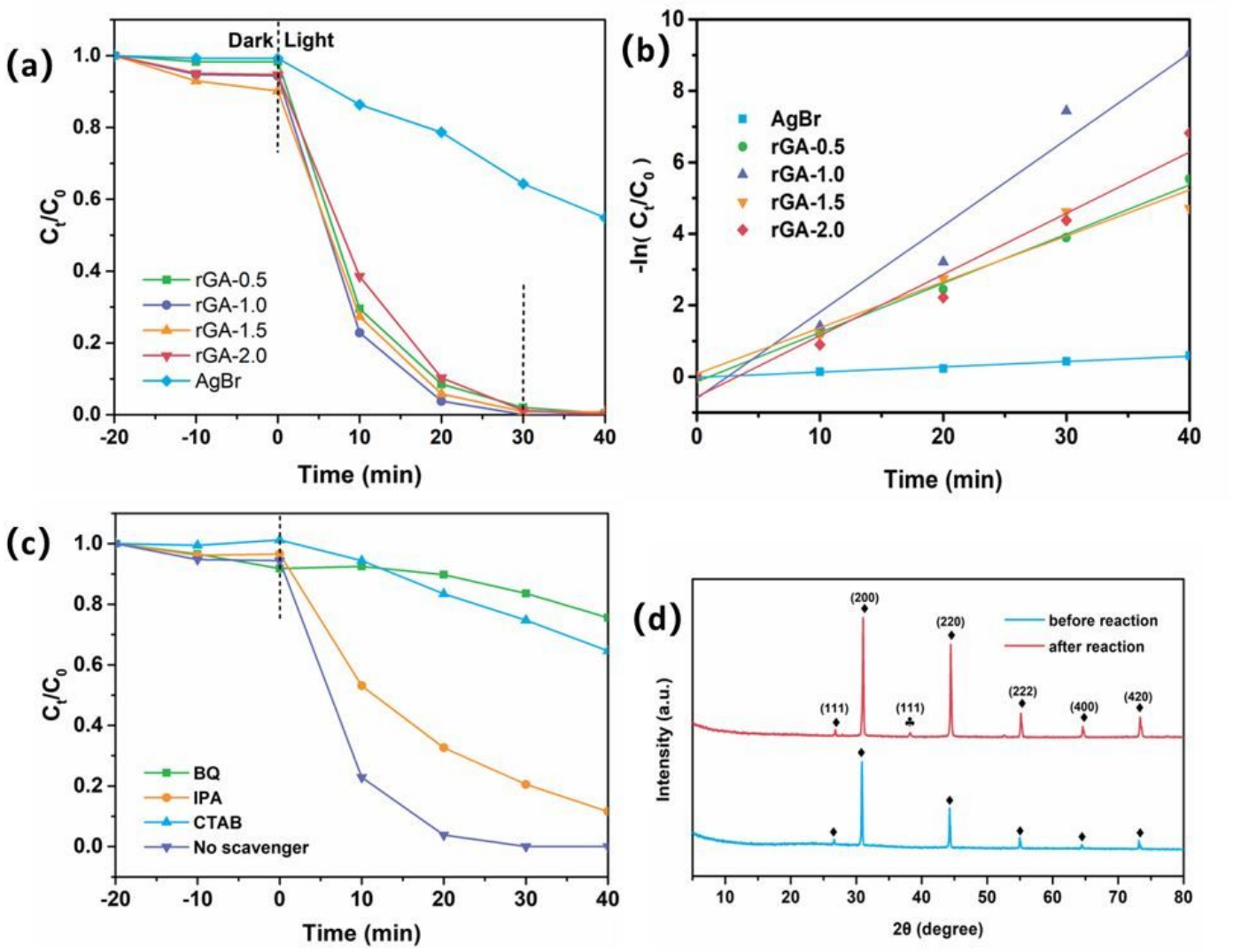

Figure 6

(a) Photocatalytic degradation and (b) photocatalytic kinetics of RhB by the AgBr and rGA-A (A=0.5, 1.0, 1.5 and 2.0) composites under visible-light irradiation; (c) the trapping experiments of rGA-1.0; (d) XRD of rGA-1.0 after the photocatalysis experiment.

Supplementary Files

This is a list of supplementary files associated with this preprint. Click to download.

- Scheme1.jpg
- Scheme2.jpg
- GraphicalAbstract.tif